2024 IEEE/RSJ International Conference on Intelligent Robots and Systems (IROS)
October 14-18, 2024. Abu Dhabi, UAE

Adaptive Control Barrier Functions for Near-Structure ROV Operations

Malte von Benzon [†*], Mathias Marley[‡], Fredrik Sørensen[†], Jesper Liniger[†], Simon Pedersen[†]
[†]Department of Energy Technology, Aalborg Univerity, Esbjerg, Denmark
[‡]Department of Marine Technology, NTNU, Trondheim, Norway
[*]Corresponding author email: msrvb@et.aau.dk

***Abstract*—This paper introduces a novel control design focused on enhancing the operational safety and efficiency of inspection, maintenance, and repair (IMR) operations conducted by autonomous remotely operated vehicles. Specifically, we propose using a safeguarding controller based on an adaptive control barrier function (CBF) incorporating safety properties previously identified in the literature. This approach permits temporary safe set violations, using an integrative penalty term to strengthen safety measures when necessary. A nominal nonlinear controller inside the safety bounds is proposed to ensure good reference tracking. The proposed controller is demonstrated in a simulation case study where an ROV (remotely operated vehicle) is set to clean an offshore monopile. The simulation includes unknown time-varying and step-like disturbances caused by water waves, the tether, ocean currents, and the high-pressure water jet. The proposed control law can react to the disturbances, and the ROV never leaves the defined safe set.**

Keywords Safety Critical Control, Adaptive CBF, UUV, ROV, Offshore Robotics, Nonlinear Control, Near-structure Operation

I. Introduction

Remotely operated vehicles (ROVs) are being used more frequently by the offshore industry to carry out underwater inspection, maintenance, and repair (IMR) tasks [1]. Automating these tasks is of great interest to the industry as it would reduce cost [2] and the dependency on skilled operators [1]. While industrial ROVs support semi-autonomous modes such as level-out and hovering [3], IMR tasks with small error tolerances close to the surface and near structures present unique challenges [2]. In academia, control of underwater vehicles is often focused on untethered vehicles operating in deep waters, such as in [4], [5]. However, near-surface operations introduce additional complexities, including the effects of the tether and surface waves [6], necessitating robust and safety-critical control strategies. In recent years, control barrier functions (CBFs) have seen a revival in safety-critical control of autonomous systems [7]. In [8], CBFs ensure safe navigation with an autonomous underwater vehicle (AUV) moving in the presence of obstacles. It is demonstrated in a test facility without external disturbances. Exponential CBF formulations for high-order safety constraints are studied in [9], whereas a more general high-order CBF (HOCBF) formulation is introduced in [10]. CBFs, or more generally HOCBFs, guarantee forward invariance of safe sets, assuming no disturbances. Robust CBF formulations [11], [12], [13] extend the safety guarantees to disturbed systems by adding a penalty term to the allowed evolution of the CBF along the undisturbed system trajectories, where the penalty term is selected based on the assumed worst-case disturbance. The conservatism of robust CBFs may be relaxed using adaptive CBF formulations [14], [15], [16], wherein an update law is used to possibly reduce the penalty term as time evolves.

This paper introduces a novel control strategy specifically designed for near-structure and near-surface autonomous ROV operations. The HOCBF formulation and notation used in [17], [18], [19] is adopted herein. In particular, this study employ a similar scheme as in [18], where two HOCBFs acting in opposite directions were used to maintain the system output within a desired range. The proposed method builds upon a nominal controller derived through Lyapunov analysis, enhanced with an adaptive disturbance estimation mechanism. The key innovation lies in developing an adaptive CBF formulation that leverages the inherent robustness of CBFs, as explored in [19]. Unlike traditional approaches that strictly enforce safety constraints within the safe set, our method permits temporary safe set violations. To manage these violations, we employ an integrative penalty mechanism that dynamically adjusts the penalty term when safety constraints are breached. Crucially, the safety constraint in the CBF design includes a robustness margin, ensuring that the system remains within a tolerable operating region even under disturbances. The effectiveness of the proposed controller is demonstrated through a case study simulating an offshore cleaning campaign on a monopile, using the specialized IMR ROV ACOMAR [20] and implemented in the ROV Simulator described in [21]. The ACOMAR model and the sensors are found through experiments.

This paper is organized as follows: Section II describes the mechanical model of the ROV, Section III presents the disturbance model, Section IV outlines the control design, and Section V evaluates the controller through a case study.

II. Mechanical model

In the following, we will distinguish between the body or b-frame and inertial or η-frame as illustrated in Fig. 1, where each frame's respective degrees of freedom are visualized.

The following assumptions, common when modeling underwater vehicles, have been used to derive the model [22], [4].

Assumption 1. *The ROV is assumed to be rigid and capable of moving in six DOF.*

Assumption 2. *The ROV is assumed symmetric about the front-back-port-starboard and the top-bottom axes.*

Assumption 3. *The body axes coincide with the principles axes of inertia. Hence, it rotates around its center of mass (COM).*

Assumption 4. *The ocean current is modeled as a constant irrotational flow in the η-frame.*

Assumption 5. *Waves are modeled as directional short-crested waves based on the JONSWAP spectrum and are projected onto the ROV by the Morrison equation, thereby assuming that the wavelength is larger than the ROV.*

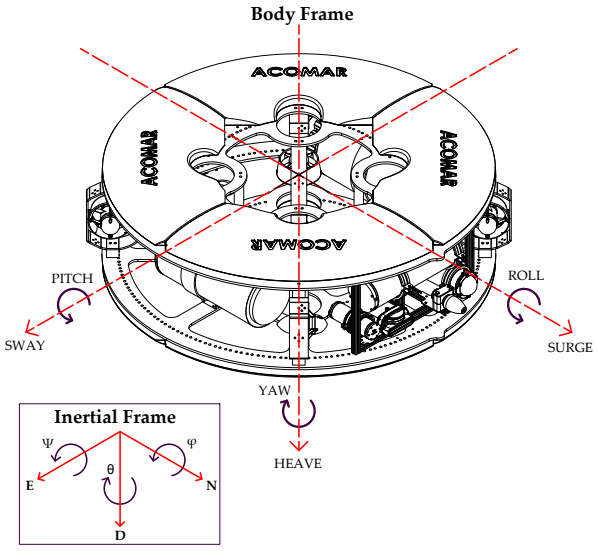

Fig. 1. The reference frame used for the analysis of ACOMAR.

The hydrodynamic model for ROVs, given in equations (1) and (2), is described by Fossen in [23], based on the vectorial form elements of the SNAME nomenclature $\boldsymbol{\eta} - \boldsymbol{\nu}$[24].

$$\dot{\boldsymbol{\eta}} = J(\boldsymbol{\eta})\boldsymbol{\nu} \tag{1}$$

$$\mathbf{M}\dot{\boldsymbol{\nu}} + \mathbf{C}(\boldsymbol{\nu})\boldsymbol{\nu} + \mathbf{D}(\boldsymbol{\nu})\boldsymbol{\nu} + \mathbf{G}(n) = \boldsymbol{\tau_t} + \boldsymbol{\tau_{dis}}. \tag{2}$$

The variables in (2) are listed in Tab. I, except for $\mathbf{G}(\boldsymbol{\eta})$ and $\mathbf{C}(\boldsymbol{\nu})$, which represent the gravitational/buoyancy force and Coriolis/centripetal forces, respectively. A description of these can be found in [23], [25]. The disturbance is denoted $\boldsymbol{\tau_{dis}}$ and consists of all external forces from the tether, water waves, and the force exerted by the cleaning tool.

Tab. I. Parameters and states.

Description	Variable	Components	Size
Mass matrix	$\mathbf{M}$	$\mathbf{M}_{\mathrm{RB}} + \mathbf{M}_{\mathrm{a}}$	6×6
Mass/Inertia	$\mathbf{M}_{\mathrm{RB}}$	$\mathrm{diag}\begin{pmatrix} m & m & m & I_x & I_y & I_z \end{pmatrix}$	6×6
Added Mass/Inertia	$\mathbf{M}_{\mathrm{a}}$	$\mathrm{diag}\begin{pmatrix} m_{a,x} & m_{a,y} & m_{a,z} & I_{a,x} & I_{a,y} & I_{a,z} \end{pmatrix}$	6×6
Thruster force	$\boldsymbol{\tau}_{\mathrm{t}}$	$\begin{pmatrix} \tau_x & \tau_y & \tau_z & \tau_\phi & \tau_\theta & \tau_\psi \end{pmatrix}^T$	6×1
Body frame velocity	ν	$\begin{pmatrix} \nu_1 & \nu_2 & \nu_3 & \nu_4 & \nu_5 & \nu_6 \end{pmatrix}^T$	6×1
Hydrodynamic drag	$\mathbf{D}$	$\begin{pmatrix} f_{d,x} & f_{d,y} & f_{d,z} & \tau_{d,\phi} & \tau_{d,\theta} & \tau_{d,\psi} \end{pmatrix}^T$	6×1

III. Disturbances

This section will briefly go through the modeling of the current, tether, and water waves that disturb the ROV working close to the surface.

Water waves are modeled as directional short-crested waves based on the JONSWAP spectrum. The JONSWAP spectrum is chosen since it is based on data collected in the North Sea, where wind turbines are placed in shallow water. The same wave model approach has been used in [26] to model waves on a different ROV. The forces from the water waves are projected onto the ROV using Morrion's equation.

The tether provides power and communication from the topside to the ROV. The tether is modeled using the lumped mass method, similar to [27] and [26]. The tether is affected by both the water waves and the current. The disturbance model acting on the ROV is given by equation (3) in η-frame,

$$\boldsymbol{\tau_{dis}} = \boldsymbol{\tau_t}(\dot{\boldsymbol{\eta}}_{\boldsymbol{w}}, \dot{\boldsymbol{\eta}}_{\boldsymbol{c}}, \dot{\boldsymbol{\eta}}_{\boldsymbol{t}}, \boldsymbol{r_t}) + \boldsymbol{\tau_w}(\dot{\boldsymbol{\eta}}_{\boldsymbol{w}}, \ddot{\boldsymbol{\eta}}_{\boldsymbol{w}}, \dot{\boldsymbol{\eta}}, \ddot{\boldsymbol{\eta}}) \tag{3}$$

where $\dot{\eta}_w$ and $\ddot{\eta}_w$ are the wave-particle velocities and accelerations, respectively. $\dot{\eta}_t$ and r_t is tether velocity and position vector respectively. The current effect is implemented as an additional velocity term that does not change in the water column. The current velocity $\dot{\eta}_c$ is given in the η-frame in equation (4).

$$\dot{\boldsymbol{\eta}}_{\boldsymbol{c}} = (\dot{N}_c, \dot{E}_c, \dot{D}_c, 0, 0, 0) \tag{4}$$

The disturbances, current velocity, and the ROV model are transported to b-frame by a rotation matrix.

IV. Control Design

A steady position in the surge direction is crucial for many IMR tasks because the tools, such as the water jet, camera, and manipulator, are often placed in the surge direction. The control design will, therefore, be focused on the surge direction, and the other directions will be stabilized on the reference by a sliding mode controller as described in [28] and [26].

A. Control design model and problem formulation

Let $x := \begin{bmatrix} \eta_1 & \nu_1 \end{bmatrix}^\top$ be the state-vector of the control design model, where η_1 denotes the position of the vehicle relative to the structure, and ν_1 is the surge velocity. Assuming the vehicle is aligned towards the structure, a simplified

model of the surge motion may be stated as the control-affine model

$$\dot{x} = f(x) + g(x)(u + \tau_{dis}), \tag{5}$$

$$f(x) := \begin{bmatrix} 0 & 1 \\ 0 & \frac{-f_{d,1}(\nu_1)\nu_1}{m+m_{a,x}} \end{bmatrix}, \quad g(x) := \begin{bmatrix} 0 \\ \frac{1}{m+m_{a,x}} \end{bmatrix}, \tag{6}$$

where τ_{dis} are the time-varying disturbances.

Let $x_{1,d}$ denote the desired vehicle surge position for optimal performance, and let $[\delta_2, \delta_1]$ specify the range of allowable surge position for safe and efficient operation, where $\delta_2 < x_{1,d} < \delta_1$.

Problem statement: **Nominal control:** For (5), design a control law u_{nom} that renders the desired point $x_d := [x_{1,d}, 0]$ asymptotically stable. **Safeguarding control:** For the system (5), design a control law that renders some set $K \subset [\delta_2, \delta_1] \times (-\infty, \infty)$ input-to-state stable.

Definition 1. $L_q H(x) = \frac{\partial H(x)}{\partial x} q(x)$ is the Lie derivative of $H(x)$ along $q(x)$. $L_q H(x)$ is used for simplicity.

Definition 2. The set K is forward invariant if for every $x_0 \in K$, $x(t) \in K$ and for $x(0) = x_0$ at $t \in [0, t_{max}]$. Then set K is a safe set with respect to the system.

An observer has been designed to estimate unknown disturbances on the ROV, such as the tool, waves, tether, and ocean currents. The observer design is given in (7).

$$\dot{\hat{\tau}}_{dis} = -a\hat{\tau}_{dis} + b(\dot{\nu}_1(m + m_{a,x}) + f_{d,1}(\nu_1)\nu_1 - u_{nom}) \tag{7}$$

The controller for the nominal will be designed based on the assumption that $\hat{\tau}_{dis} \approx \tau_{dis}$.

B. Design of Nominal Control

Now, consider the Lyapunov function candidate,

$$V(\sigma) = 0.5\sigma^2 \tag{8}$$

where σ defined by (9) is a linear combination of the error defined in (10) and the error dynamics defined in (11). $c_0 > 0$ ensures stability of σ. (8) is positive-definite such that $V(\sigma) \to \infty$ for $\sigma \to \infty$.

$$\sigma = \dot{e} + c_0 e \tag{9}$$

$$e = x_{1,d} - x_1 \tag{10}$$

$$\dot{e} = x_{2,d} - x_2 \tag{11}$$

To ensure the asymptotic stability of the nominal controller, $\dot{V}(\sigma)$ must be negative semi-definite, such that $\dot{V}(\sigma) < 0 \; \forall \; \sigma \neq 0$. $\dot{V}$ is bounded, which can be expressed as (12), where $\alpha > 0$. As long as the derivative of (8) is upper bounded by (12) (input bounded). Then the derivative of (8) is decrescent, and since (12) is negative definite $\sigma = 0$ is stable.

$$\dot{V}(\sigma) = -\alpha\sqrt{V(\sigma)} \tag{12}$$

The time derivative of (8) is seen in (13). From this, a control law can be derived.

$$\dot{V}(\sigma) = \sigma\dot{\sigma} \tag{13}$$

Inserting (9) in (13) leads to (14).

$$\dot{V}(\sigma) = \sigma(\dot{x}_{2,d} - f(x) - g(x)u_{pd} + c_0\dot{e}) \tag{14}$$

By looking at the right-most bracket of (14) and setting it equal to (12), the control law u is derived to be (15).

$$u_{pd} = g(x)^{-1}(\dot{x}_{2,d} + \dot{e}(c_0 + \frac{\alpha}{\sqrt{2}}) + e\frac{\alpha c_0}{\sqrt{2}} - f(x)) \tag{15}$$

The control law in (15) alters (14) negative-semi definite shown in (16) and thereby the system described in (5) with the controller (15) is asymptotically stable. For simplicity we define $k_d = (c_0 + \frac{\alpha}{\sqrt{2}})$ and $k_p = \frac{\alpha c_0}{\sqrt{2}}$.

$$\dot{V}(\sigma) = \sigma(-\frac{\alpha}{\sqrt{2}}\sigma) \tag{16}$$

The controller defined within the safe set will then be,

$$u_{nom} = u_{pd} + \hat{\tau}_{dis} \tag{17}$$

C. Safeguarding control law

In severe waves, the nominal controller by itself may not be able to maintain the ROV within a safe distance to the structure. We use CBF theory to design a nonlinear control law that increases the magnitude of the commanded control inputs if the ROV deviates far from the desired setpoint.

Define the second-order CBF

$$B_1^f(x) := x_1 - \delta_1 \tag{18}$$

$$B_2^f(x) := L_f B_1^f(x) + B_1^f(x)/T_1 \tag{19}$$

where δ_1 specifies a safe distance to the structure, T_1 is a time constant, and f denotes forward direction. Let B_1^f and B_2^f define the safe sets $K_1^f := \{x : B_1^f(x) \leq 0\}$, $K_2^f := \{x : B_2^f(x) \leq 0\}$, and $K^f := K_1^f \cap K_2^f$. Noting that $x \in K_2^f \implies \dot{B}_1^f = L_f B_1^f(x) \leq -B_1^f(x)/T_1$, solutions cannot leave K_1^f while inside K_2^f. For the undisturbed system, any control input u satisfying $\dot{B}_2^f = L_f B_2^f(x) + L_g B_2^f(x)u \leq -B_2(x)/T_2$ will render K_2^f forward invariant, and thereby K^f, forward invariant. As an additional safety measure towards disturbances, we select the safe input set as

$$U_f(x) := \{u : L_f B_2(x) + L_g B_2(x)u \leq -\frac{B_2(x)}{T_2} - \gamma\}, \tag{20}$$

where γ is a penalty term with update law

$$\begin{aligned} \dot{\gamma} :=& \Gamma(x, \gamma) \\ =& k_1 \min(0, B_2^f(x)) \\ &+ k_2 \max(0, B_2^f(x)) + k_3 \max(0, B_1^f(x)). \end{aligned} \tag{21}$$

The key idea behind the update law Γ is that the allowed set of control inputs shrinks whenever $x \notin K^f$, and may grow when $x \in K^f$.

To ensure good performance, it is desired that the ROV does not drift away from the structure, defined by δ_2. To this end, we use another HOCBF

$$B_1^b(x) := -x_1 - \delta_2 \tag{22}$$

$$B_2^b(x) := L_f B_2^b(x) + B_2^b(x)/T_3 \tag{23}$$

to define another safe input set

$$U_b(x) := \{u : L_f B_2^b(x) + L_g B_2^b(x) u \leq -\frac{B_2^b(x)}{T_4}\}, \tag{24}$$

where superscript b denotes backward direction. Finally, the control law can be defined as,

$$\kappa_s(x) := \arg \min_{u \in U_f(x) \cap U_b(x)} |u - u_{nom}|. \tag{25}$$

Let K_1^b and K_2^b be the zero sublevel sets of B_1^b and B_2^b respectively, and define the safe sets $K^b := K_1^b \cap K_2^b$ and $K := K^f \cap K^b$. Using the results of [19], it may be verified that the disturbed system

$$\dot{x} = f(x) + g(x)(\kappa_s(x) + \tau_{dis}) \tag{26}$$

is input-to-state stable with respect to K.

V. Case Study

The case study to evaluate the controller will be based on a simulation of a marine growth cleaning campaign with the specialized ROV ACOMAR presented in [20]. Marine growth such as alleges and mussels increases the weight and the loads on offshore structures and prohibits crack detection [29]. In this simulation study, the controlled ROV will be set to clean a structure from 20-5 m in depth. The cleaning tool will be a high-pressure water jet that exerts a constant force of $150\,\mathrm{N}$ in the surge direction. This corresponds to the reaction force from a typical cleaning flow. The waves will have a significant wave height of 1.8 m with a wave period of 6.75 sec, and the ocean current is 0.2 m/s from a northwest direction. These are typical sea state conditions. Tab. II shows the wave and tether constants. An explanation of these can be found in [26].

Tab. II. Wave and tether constants used for simulations

Notation	Value	Unit	Obtained from
c	2	-	[30]
d	50	m	North Sea data
γ	3.3	-	JONSWAP
ζ	-0.7854	rad	North Sea data
m_{tet}	0.043	kgm^{-1}	Experimental
d_{tet}	0.033	m	Experimental
Cn_{tet}	1.2	–	[31]
Ct_{tet}	0.01	–	[31]
C_{tet}	100	Nsm^{-1}	[31]
E_{tet}	$6.4{\cdot}10^{10}$	N/m^2	[31]
l_0	35	m	Determined

The model parameters for the ROV are shown in Tab. III, and the hydrodynamic drag forces/torques are shown in Tab. IV.

Tab. III. Constants for ACOMAR.

Description	Parameter	Value	Unit
Mass	m	133.94	kg
Added mass	$(m_{a,x}, m_{a,y}, m_{a,z})$	123.42, 123.42, 311.80	kg
Moment of inertia	I_{xx}, I_{yy}, I_{zz}	19.97, 20.53, 30.08	kgm^2
Added inertia	$(I_{a,x}, I_{a,y}, I_{a,z})$	133.94	kg
Dimensions	L, H, W	0.46, 0.38, 0.58	m
Volume	$\forall$	0.134	m^3
Distance from COM to COB	r_g^b	0.012	m
Gravity acceleration	g	9.82	$\frac{m}{s^2}$
Water density	ρ	1000	$\frac{kg}{m^3}$

Tab. IV. Drag force/torque equations.

Motion	Drag force/torque
Surge	$f_{d,x} = 189.5\|\nu_1\| + 31.17$
Sway	$f_{d,y} = 189.5\|\nu_2\| + 31.17$
Heave	$f_{d,z} = 900.1\nu_3^2 + 371.3\|\nu_3\|$
Roll	$\tau_{d,\phi} = 237.9\|\nu_4\|$
Pitch	$\tau_{d,\theta} = 237.9\|\nu_5\|$
Yaw	$\tau_{d,\psi} = 237.9\|\nu_6\|$

No theoretical guarantees have been given to prove that $\hat{\tau}_{dis}$ converges to τ_{dis} therefore, a simulation study is performed to show that the estimator converges to the actual value; this is shown in Fig. 2. In Fig. 2(a), a step-like disturbance from the water jet turned on at 5 sec. The estimated value converges toward the actual value with a small steady-state error in 0.5 sec. In Fig. 2(b), a time-varying water wave causes the disturbance. The estimator is initialized at 0, where the actual value is 51 N. The estimated value converges to the actual value in 0.3 sec and afterward follows the wave disturbance with a small error. In Fig. 2(c), the disturbances are caused by waves, current, tether, and the water jet. The waves, current, and tether affect the ACOMAR from the beginning, and the water jet is turned on at 20 sec. Before it is turned on, the error is on par with the wave estimate shown in Fig.2(b). After the water jet is turned on, the error between the estimated and actual values gets larger and fluctuates more. However, the estimate still converges to the actual disturbance as proposed in the control design.

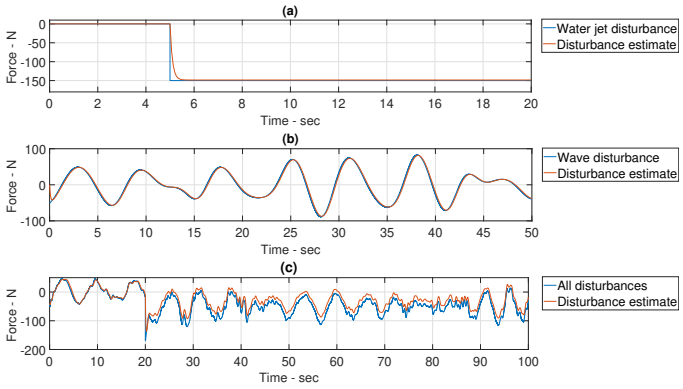

Fig. 2. Open-loop disturbance estimate and actual disturbance, the ACOMAR is initialized at 10 m in depth. (a) a constant step-like disturbance of 150 N from the water jet, (b) wave disturbance with a significant wave height of 2 m, and (c) wave, tether, current of 0.1 m/s, and the water jet turned on at 20 sec. The tether and wave parameters can be found in Tab. II. It should be noted that the range of the time axis is different between the plots.

The references and initial conditions in the simulation will be zero for the sway motion and all the angles such that $\eta_2, \eta_4, \eta_5, \eta_6 = 0$. The reference for $\eta_1 = -0.1$m with initial condition $\eta_1(0) = -0.2$m. In heave, the ROV will move with a constant velocity of $\nu_3 = 0.06$m/s and $\eta_3(0) = 20$m. The initial velocity is zero for all motions. The high-pressure water jet is turned on after 20 sec. The sensor feedback in the simulation includes realistic noise measured from the ACOMAR, and the sampling period is set to 15 Hz, which is limited by the actual feedback on the ROV.

The safe set defined by $[\delta_2, \delta_1]$ will be chosen as $[\delta_2 = -0.15\text{m}, \delta_1 = -0.08\text{m}]$, note that the ROV will initialized outside the safe set. The tuning parameters for the controller are shown in Tab. V

Tab. V. Tuned control parameters

Parameter	T_1, T_3	T_2, T_4	k_1	k_2	k_3	k_p	k_d	$\gamma(0)$
Value	0.01	0.4	0.01	25	100	10	3.17	1

A. Results

Fig. 3 and 4 shows the simulation results. In Fig. 3(a), we observe that the surge position remains within the set $[\delta_2, \delta_1]$, even when the disturbances shown in Fig. 3(b) and 3(c) gets larger close to the surface, this means that the state of the system (5) remains within the set K_1. Yet, as is shown in Fig. 4(b), the penalty term γ increases above zero. This is because the update law Γ takes both position and velocity into account, implicitly through B_1 and B_2. Thus, γ increases when solutions leave K_2, which must happen before solutions leave K_1. This feature enables the proposed adaptive CBF formulation to react to sudden disturbances quickly, thus obtaining improved disturbance rejection compared to linear proportional-integral-derivative controllers where only the positional error is used as input to the integral action. The quick reaction time is shown at 20 sec when the water jet is turned on as a step disturbance. It is barely visible in surge position Fig. 3(a), but it can be seen clearly on the input to the ROV shown in Fig. 4(a) where the corresponding water jet force offsets the input force. Even though the ROV is initialized outside the safe set, the safeguarding controller returns it to the reference. The controller activity can be seen in Fig. 4(c). The safeguarding controller is activated more frequently when moving closer to the surface. The increased disturbances from waves and the tether cause this. When comparing the proposed controller to simulations with only the nominal controller, the error gets larger, and the ROV does not keep within the optimal cleaning range. Due to limitations on space, these results are not included in this paper but will be included in a future paper.

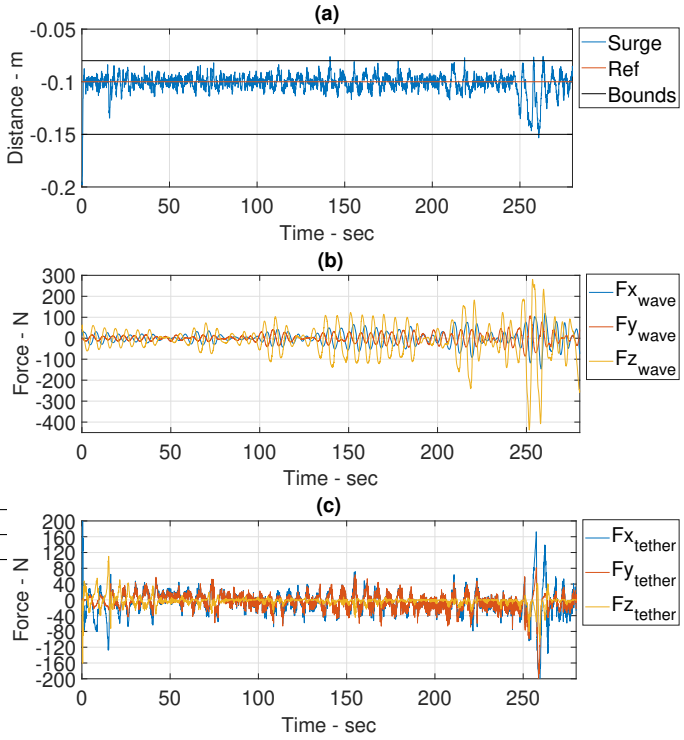

Fig. 3. (a) shows the surge position, (b) shows the wave forces, and (c) shows the tether forces.

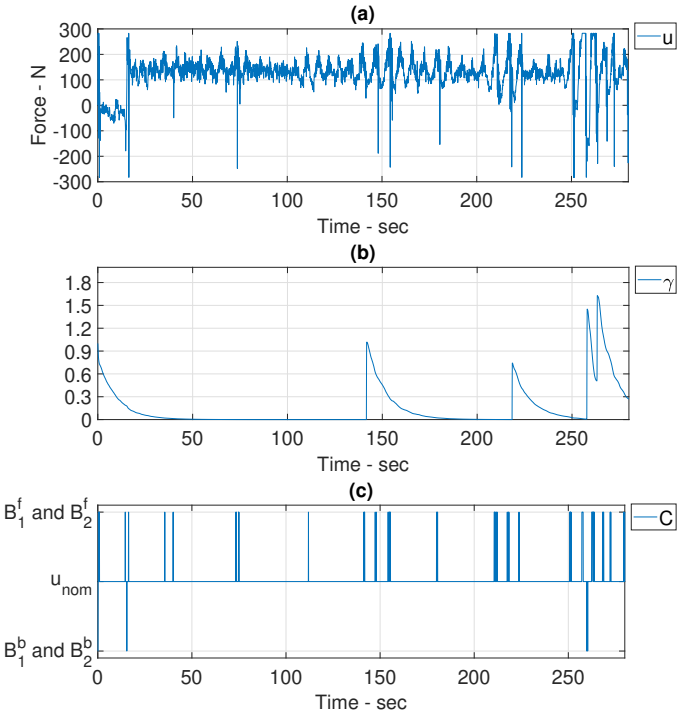

Fig. 4. (a) shows the input force in the surge direction, (b) shows the evolution of γ, and (c) shows the control activity C.

VI. Conclusion

We have proposed a control strategy based on a nominal and safeguarding controller for performing autonomous IMR tasks with ROVs close to the surface and near offshore structures. The proposed safety controller utilizes CBFs to design a nonlinear control law that increases the control input if the ROV leaves the desired setpoint. As an additional safety measure, a penalty term is added that shrinks when the ROV is inside the safe set and grows when it leaves. The pro-

posed safety controller is demonstrated in a simulation case study where an ROV is set to clean an offshore monopile. The simulation includes disturbances from water waves, the tether, ocean currents, and the high-pressure water jet. The proposed control law is able to react to the disturbances, and the ROV never leaves the defined safe set.

VII. Future work

Preliminary results not presented here have shown that compared to the sliding mode control in [28], the proposed controller reduces input chatter while keeping a similar overall performance. A more in-depth comparative study should be performed to demonstrate the usefulness of the proposed controller. This should also include a comparison to other CBF approaches. One limitation of the demonstrated case study is that the wave model is stochastic. Therefore, this paper has yet to demonstrate that the proposed method can handle specific operational conditions, only that it handles the disturbances shown. A comprehensive simulation study, where the sea state is reevaluated, must be performed to conclude the usefulness of the proposed controller in certain operating conditions. Moreover, experimental testing should be performed to further demonstrate the proposed controller's performance with IMR tasks.

References

[1] I. Tena, "Automating rov operations in aid of the oil & gas offshore industry," Tech. Rep., 2011. [Online]. Available: https://www.unmannedsystemstechnology.com/wp-content/uploads/2013/10/White-Paper-Automating-ROV-Operations.pdf

[2] A. Shukla and H. Karki, "Application of robotics in offshore oil and gas industry— a review part ii," *Robotics and autonomous systems*, vol. 75, pp. 508–524, 2016. [Online]. Available: https://search.datacite.org/works/10.1016/j.robot.2015.09.013

[3] C. Mai, S. Pedersen, L. Hansen, K. Jepsen, and Z. Yang, "Modeling and control of industrial rov's for semi-autonomous subsea maintenance services," *IFAC-PapersOnLine*, vol. 50, no. 1, pp. 13 686–13 691, 2017, 20th IFAC World Congress. [Online]. Available: https://www.sciencedirect.com/science/article/pii/S2405896317334572

[4] S. J. Ohrem, H. B. Amundsen, W. Caharija, and C. Holden, "Robust adaptive backstepping dp control of rovs," *Control Engineering Practice*, vol. 127, p. 105282, 2022. [Online]. Available: https://www.sciencedirect.com/science/article/pii/S0967066122001393

[5] L. G. García-Valdovinos, T. Salgado-Jiménez, M. Bandala-Sánchez, L. Nava-Balanzar, R. Hernández-Alvarado, and J. A. Cruz-Ledesma, "Modelling, design and robust control of a remotely operated underwater vehicle," *International Journal of Advanced Robotic Systems*, vol. 11, no. 1, 2014.

[6] K. L. Walker, A. A. Stokes, A. Kiprakis, and F. Giorgio-Serchi, "Feed-forward disturbance compensation for station keeping in wave-dominated environments," in *OCEANS 2023 - Limerick*, 2023, pp. 1–7.

[7] A. D. Ames, S. Coogan, M. Egerstedt, G. Notomista, K. Sreenath, and P. Tabuada, "Control barrier functions: Theory and applications," in *2019 18th European Control Conference (ECC)*, 2019, pp. 3420–3431.

[8] C. Wang, W. Yu, S. Zhu, L. Song, and X. Guan, "Safety-critical trajectory generation and tracking control of autonomous underwater vehicles," *IEEE Journal of Oceanic Engineering*, vol. 48, no. 1, pp. 93–111, 2023.

[9] Q. Nguyen and K. Sreenath, "Exponential control barrier functions for enforcing high relative-degree safety-critical constraints," in *Proc. American Control Conf.* Boston, MA, USA: American Automatic Control Council (AACC), 2016, pp. 322–328.

[10] W. Xiao and C. Belta, "High-Order Control Barrier Functions," *IEEE Transactions on Automatic Control*, vol. 67, no. 7, pp. 3655–3662, 2022.

[11] Y. Emam, P. Glotfelter, and M. Egerstedt, "Robust barrier functions for a fully autonomous, remotely accessible swarm-robotics testbed," in *Proc. IEEE Conf. Decision and Control*, Nice, France, 2019, pp. 3984–3990.

[12] Q. Nguyen and K. Sreenath, "Robust safety-critical control for dynamic robotics," *IEEE Transactions on Automatic Control*, vol. 67, no. 3, pp. 1073–1088, 2022.

[13] K. Garg and D. Panagou, "Robust Control Barrier and Control Lyapunov Functions with Fixed-Time Convergence Guarantees," in *Proc. American Control Conf.*, New Orleans, LA, USA, 2021, pp. 2292–2297.

[14] A. J. Taylor and A. D. Ames, "Adaptive safety with control barrier functions," in *Proc. American Control Conf.*, Denver, CO, USA, 2020, pp. 1399–1405.

[15] M. Maghenem, A. J. Taylor, A. D. Ames, and R. G. Sanfelice, "Adaptive safety using control barrier functions and hybrid adaptation," in *Proc. American Control Conf.*, New Orleans, LA, USA, 2021, pp. 2414–2419.

[16] B. T. Lopez, J. J. E. Slotine, and J. P. How, "Robust Adaptive Control Barrier Functions: An Adaptive and Data-Driven Approach to Safety," *IEEE Control Systems Letters*, vol. 5, no. 3, pp. 1031–1036, 2021.

[17] M. Marley, R. Skjetne, E. Basso, and A. R. Teel, "Maneuvering with safety guarantees using control barrier functions," *IFAC-PapersOnLine*, vol. 54, no. 16, pp. 370–377, 2021. [Online]. Available: https://www.sciencedirect.com/science/article/pii/S2405896321015202

[18] M. Marley and R. Skjetne, "Mitigating Force Oscillations in a Wave Energy Converter Using Control Barrier Functions," ser. International Conference on Offshore Mechanics and Arctic Engineering, vol. Volume 8: Ocean Renewable Energy, 06 2022, p. V008T09A089. [Online]. Available: https://doi.org/10.1115/OMAE2022-82707

[19] M. Marley, R. Skjetne, and A. R. Teel, "Sufficient conditions for uniform asymptotic stability and input-to-state stability using high-order control barrier functions," *IEEE Transactions on Automatic Control*, vol. 69, no. 4, pp. 2352–2366, 2024.

[20] C. Mai, M. v. Benzon, F. F. Sørensen, S. S. Klemmensen, S. Pedersen, and J. Liniger, "Design of an autonomous rov for marine growth inspection and cleaning," in *2022 IEEE/OES Autonomous Underwater Vehicles Symposium (AUV)*, 2022, pp. 1–6.

[21] M. von Benzon, F. F. Sørensen, E. Uth, J. Jouffroy, J. Liniger, and S. Pedersen, "An open-source benchmark simulator: Control of a bluerov2 underwater robot," *Journal of Marine Science and Engineering*, vol. 10, no. 12, 2022. [Online]. Available: https://www.mdpi.com/2077-1312/10/12/1898

[22] G. Antonelli, *Underwater Robots*. Springer Cham, 2018.

[23] T. Fossen, *Handbook of Marine Craft Hydrodynamics and Motion Control*. Wiley, 2021.

[24] SNAME: The Society of Naval Architects and Marine Engineers, "Nomenclature for treating the motion of a submerged body through a fluid," *Technical and Research Bulletin No. 1-5*, 1950.

[25] C. S. Chin and M. Lau, *Benchmark Models of Control System Design for Remotely Operated Vehicles*. Springer Singapore, 2020.

[26] M. von Benzon, J. Liniger, F. F. Sørensen, and S. Pedersen, "Investigation of operating range of marine growth removing rov under offshore disturbances," *IFAC-PapersOnLine*, vol. 55, no. 31, pp. 85–90, 2022, 14th IFAC Conference on Control Applications in Marine Systems, Robotics, and Vehicles CAMS 2022. [Online]. Available: https://www.sciencedirect.com/science/article/pii/S2405896322024594

[27] M. D. Masciola, M. Nahon, and F. R. Driscoll, "Static analysis of the lumped mass cable model using a shooting algorithm," *Journal of Waterway, Port, Coastal, and Ocean Engineering*, 2012.

[28] M. von Benzon, F. Sørensen, J. Liniger, S. Pedersen, S. Klemmensen, and K. Schmidt, "Integral sliding mode control for a marine growth removing rov with water jet disturbance," in *2021 European Control Conference (ECC)*, 2021, pp. 2265–2270.

[29] I. Jusoh and J. Wolfram, "Effects of marine growth and hydrodynamic loading on offshore structures," 1996. [Online]. Available: https://api.semanticscholar.org/CorpusID:108015670

[30] DNV (Det Norske Veritas), "Environmental conditions and environmental loads," 2021.

[31] E. C. De Souza and N. Maruyama, "Intelligent uuvs: Some issues on rov dynamic positioning," *IEEE Transactions on Aerospace and Electronic Systems*, vol. 43, no. 1, pp. 214–226, 2007.